Mechanoluminescence of (Eu, Ho)-doped oxynitride glass-ceramics from the BaO-SiO2-Si3N4 chemical system

Alexis Duval, Patrick Houizot, Xavier Rocquefelte, Tanguy Rouxel

Mechanoluminescence of (Eu, Ho)-doped oxynitride glass-ceramics from the BaO-SiO_2-Si_3N_4 chemical system

Alexis Duval[a], Patrick Houizot[a], Xavier Rocquefelte[b] and Tanguy Rouxel[a,c*]

[a]Glass Mechanics Dept., IPR, UMR 6251, University of Rennes, Campus de Beaulieu, 35042 Rennes cedex, France.

[b]ISCR, UMR 6226, University of Rennes, Campus de Beaulieu, 35042 Rennes cedex, France.

[c]Institut Universitaire de France.

*corresponding author: tanguy.rouxel@univ-rennes1.fr

Abstract — Mechanoluminescence is observed in oxynitride glass-ceramics from the BaO-SiO_2-Si_3N_4 chemical system, doped with Eu and Ho. Light emission was investigated by means of uniaxial compression experiments on disks and parallelepipedic bars with constant loading rates ranging from 0.3 to 300 $MPa.s^{-1}$ up to about 500 MPa. In agreement with previous reports on $SrAl_2O_4$-based materials[1,2], the mechanoluminescence intensity is found proportional to the mechanical power. Nevertheless, in contrast with $SrAl_2O_4$, no gain in the intensity is observed at the onset of the unloading stage, but a drop of the photoluminescence intensity during unloading. This stems from different electron trapping populations and associated energy levels for the $Ba_4Si_6O_{16}$ phase (the dominant crystallized phase in the present glass-ceramics), which are discussed in the light of *DFT* calculations.

Various materials, organic[3] and inorganic[4], are known to emit light when submitted to a mechanical loading. For example, this is the case of Eu-doped $SrAl_2O_4$ whose luminescence and mechanoluminescence properties were studied in the 1990s [5] [6]. This phenomenon is referred to as mechanoluminescence, and includes elastico-mechanoluminescence, plastico-mechanoluminescence, and fracto-mechanoluminescence[7]. In general, mechanoluminescence is observed by grinding or compressing a composite material containing the active crystallized phase after exposure to *UV* light[1,2,6]. Mechanoluminescence was recently reported in a germanate-based glass-ceramic doped with Cr^{3+} by means of ball-dropping experiments performed on powder[8], and in Pr^{3+}-doped borate-based glass-ceramic/epoxy composites using compression experiments [9]. The mechanoluminescence of Eu^{2+}-doped ceramics such as $BaSi_2O_2N_2$[10] or $BaAl_2Si_2O_8$[11] has been known for about three decades. Several studies were dedicated to the luminescent properties of $Ba_4Si_6O_{16}$:Eu^{2+}, *RE* (*RE* = rare-earth) ceramics[12,13,14,15]. In these crystalline phases, *RE* substitutes for Ba thanks to close ionic radii[16], so as to keep the (Ba+Eu+*RE*)/Si ratio constant and equal to 2/3.

Interest in the $Ba_4Si_6O_{16}$ composition also lies in its ability to vitrify and further result in a glass-ceramic through a congruent crystallization of the parent glass[17]. In the present study, we show that the $Ba_4Si_6O_{16}:Eu^{2+}$, Ho^{3+} crystal, while being centrosymmetric, exhibits mechanoluminescence.

In this work, a barium-silicate glass was doped with a mixture of (Eu, *RE*) elements, and some nitrogen is further incorporated to control the oxidation state of europium. The doped-glass was further crystallized by heat-treatment and the mechanoluminescence intensity was then studied by means of compressive experiments on centimeter size bulk specimens. The *RE* element was chosen so as to optimize the mechanoluminescence intensity of the main crystallized phase, namely $Ba_4Si_6O_{16}:Eu^{2+}$, *RE*. In order to reach this objective, $Ba_4Si_6O_{16}:Eu^{2+}$, *RE* containing 3 cat. % Eu and 2 cat. %. *RE* (*RE* = Sc, Y, La, Ce, Pr, Nd, Sm, Eu, Gd, Tb, Dy, Ho, Er, Tm, Yb or Lu) ceramics were first synthesized, starting from dried $BaCO_3$ (Sigma-Aldrich, 99%), Gd_2O_3, Lu_2O_3, Dy_2O_3, Sc_2O_3, Eu_2O_3 (Sigma-Aldrich, 99.9%), SiO_2 (Sigma-Aldrich, 99.5%), Pr_2O_3 and Sm_2O_3 (Fischer 99.9 %), Tb_4O_7 (Fischer 99.998 %), Tm_2O_3 (Alfa Aesar 99.9 %), Yb_2O_3, La_2O_3, CeO_2, Nd_2O_3 (Rhône-Poulenc 99.99 %), Y_2O_3 (Acros 99.99 %), and Ho_2O_3 Er_2O_3 (Rhône-Poulenc 99.999%). These *RE* concentrations were selected so as to optimize the intensity of the mechanoluminescence. Stoichiometric amounts were weighted and hand-grounded during 15 minutes with a small amount of ethanol in an agate mortar, and then fired 6 h at 1300 °C in a N_2:H_2 = 94:6 reducing atmosphere in order to favor europium in the 2+ oxidation state. The obtained ceramic powders were added to an epoxy resin with a final ceramic content of 20 wt. % (≈ 6 vol. %), and ceramic/epoxy composites disks, 11.5 mm diameter and 6 mm thick, were shaped. Then, an oxynitride glass with a 36.7BaO-57.6SiO_2-1.7Si_3N_4-3.0 EuO-1.0Ho_2O_3 molar composition was synthesized, starting from dried precursors. The oxide powders were mixed together and dried at 1200 °C for 5 h. The resulting mixture (about 40 g) was grounded with a Si_3N_4 powder (Sigma-Aldrich, 99.9%) in an agate mortar. The mixture was then heated in a BN crucible placed inside an atmosphere-controlled apparatus containing both furnaces for melting and annealing, with a nitrogen pressure of 1 atm (see ref.[18] for details). The powder mixture was melted at 1600 °C and further annealed at T_g-50 °C (T_g = 737 °C) for 3 h. Note that the glass was crushed and re-melted thrice to get a homogeneous glass batch. Glass-ceramics were obtained by heat-treating the glass in a nitrogen atmosphere at temperatures between 857 and 1200 °C, as is discussed further in relation to the optical properties. The X-ray diffraction (*XRD*) patterns were recorded using a PANalytical X'pert Pro diffractometer using Cu-Kα radiation (1.5418 Å). Mechanical experiments were performed on the ceramic/epoxy composite disks (diametral compression test) and on 4x4x5 mm^3 parallelepipedic specimens, mirror-polished (1 µm diamond suspension), for the glass-ceramics, using a Schimadzu-AGS-X testing machine equipped with a 10 kN load cell and a SiC pusher. In the case of diametral compression, the maximum tensile

stress is located at the center of the composite and is expressed as $\sigma = \frac{2P}{\pi dh}$, where P is the load, d is the diameter and h is the thickness of the cylindrical composites[19]. Although the "elastic" stress at - and immediately adjacent to - the contact areas with the SiC plates is larger (see the red dots at the bottom right of Fig. 1c), the stress gradient is too large and the contact area is too small to attribute the light emitted in this region to a particular stress value. Nevertheless, this requires additional investigations because it is not excluded that the compressive and tensile stresses lead to different phenomena. The luminescence intensity was measured using a Zyla 5.5 sCMOS Andor Technology high sensitivity camera. Samples were irradiated for 2 minutes with a 365 nm *UV* light prior to each measurement. The Density Functional Theory (*DFT*) calculations on the $Ba_4Si_6O_{16}$ crystal (a = 12,477 Å, b = 4,685 Å, c = 13,944 Å and β = 93.54° [20]) were performed at ambient pressure using the *VASP* code (Vienna ab-initio Simulation Package; www. vasp.at) [21] [22]. This code allows to determine the ground state properties of a given compound based on *DFT* calculations and is based on a plane wave based Projector Augmented Wave (*PAW*) approach. The semi-local Perdew–Burke–Ernzerhof (*PBE*) functional [23] on a (a,3b,c) supercell containing 156 atoms was used to identify the defect energy levels responsible for the detrapping processes. The wavefunctions were expanded in plane waves up to a kinetic energy cut-off of 500 eV, and the k-point sampling was chosen sufficiently fine to ensure the numerical convergence of all the calculated properties. In particular, the accurate calculation of the total energy for all defect models (155 atoms supercell) was carried out using a 6 × 6 × 6 k-point mesh. The geometry was optimized until the forces on all the atoms were less than $3 \cdot 10^{-2}$ eV $Å^{-1}$.

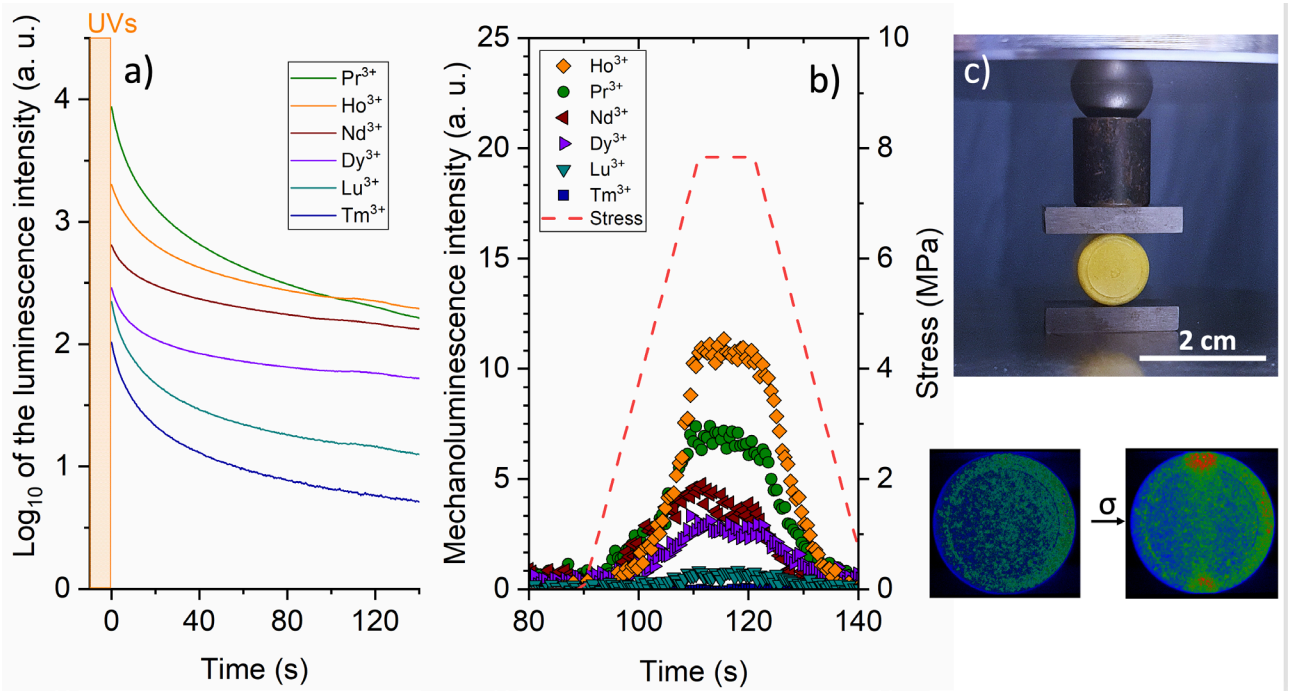

FIG. 1. a) Luminescence decay and b) mechanoluminescence of some of the synthesized $Ba_4Si_6O_{16}:Eu^{2+}$, *RE* ceramic/epoxy composites, c) photograph of the experimental setup and camera photograph of the composite before and during the diametral compression test. The mechanoluminescence is evidenced by a stronger luminescence. Note that for sake of clarity, curves obtained on grades containing Sc, Y, La, Ce, Sm, Eu, Gd, Tb, Er, or Yb were not drawn.

In a first stage, the $Ba_4Si_6O_{16}:Eu^{2+}$, *RE* ceramic/epoxy disks were irradiated with a *UV* light for 2 min and were further submitted to diametral compression experiments, 90 s later, following the same experimental procedure for each grade. Results regarding the phosphorescence decay following the irradiation show that Pr, Ho and Nd are the three best candidates in terms of luminescence intensity (Fig. 1a). However, the mechanoluminescence signal observed after 90 s as a mechanical loading cycle is applied gives a clear advantage to Ho co-doping (Fig. 1b). The spatial distribution of the mechanoluminescence signal is consistent with the stress field associated with a diametral compression specimen, i.e. with a maximum tensile stress in the center of the disk and maximum compressive stresses beneath the area of contact with the upper and lower pistons (Fig. 1c). In regard of these preliminary investigations, a barium-silicate glass containing europium and holmium with a (Ba+Eu+Ho)/Si ratio equal to 2/3, as in the $Ba_4Si_6O_{16}$ crystal, was synthesized in a second stage. Nevertheless, in order to promote Eu in the 2+ oxidation state, some nitrogen is incorporated using Si_3N_4 as a starting powder. This results in a more durable, harder and stiffer glass with the following composition: 36.7 BaO-57.6 SiO_2-1.7 Si_3N_4-3.0 EuO-1.0 Ho_2O_3, or $Ba_{13.6}Si_{23.3}Eu_{1.12}Ho_{0.75}O_{58.7}N_{2.53}$. The increase of the Eu^{2+}/Eu^{3+} ratio with the nitrogen content was already observed by Ramesh et al.[24], and confirmed both by *LECO* measurements and by measuring the emission spectra of the glass, where the characteristic broadband emission of Eu^{2+} was outlined [25]. The chemical reaction involved in this process is written as

$$Si_3N_4 + 6\ Eu_2O_3 \rightarrow 3\ SiO_2 + 12\ EuO + 2\ N_2 \qquad (1)$$

and is thermodynamically feasible above 1480 K[26,27]. The obtained glass is homogeneous to the naked eyes and has an amber color (Fig. 2), which is typically observed in glasses with over 0.2 at. % of europium in its divalent state[25]. A nitrogen content of 6 eq. % N is required to reach a nearly complete reduction of Eu^{3+}. The nucleation and growth of crystals from an oxide-glass having the same cationic composition as the presently prepared oxynitride glass was previously studied[17]. The density of crystals, which is of the order of 10^{12} crystals·m^{-3} within a few hours, increased slightly with the holding time at T_g+20 °C. In the case of silicon oxynitride glasses, the partial decomposition of silicon nitride into metallic silicon (or silicides with impurities) and molecular nitrogen leads to the formation of homogeneously distributed metallic Si-based nano-size particles [28,29,25]. This situation promotes a uniform crystallization process from these particles, resulting in the growth of dendrites from the

metallic nuclei (Fig. 2a) and in a considerably larger density of crystals (about 10^{15} crystals·m^{-3}) than in the parent oxide glass. Besides, a nucleation step is no more necessary as, in general, oxynitride glasses appear to be self-nucleating[26]. Nitrogen in the glass network induces i) the reduction of Eu^{3+} into Eu^{2+}, which is of primary importance to observe the long-lasting phosphorescence and mechanoluminescence of the glass-ceramics, ii) the formation of micro and nano-sized intermetallic particles tremendously increasing the ease for a uniform crystallization, and iii) the improvement of the corrosion resistance and the mechanical properties.

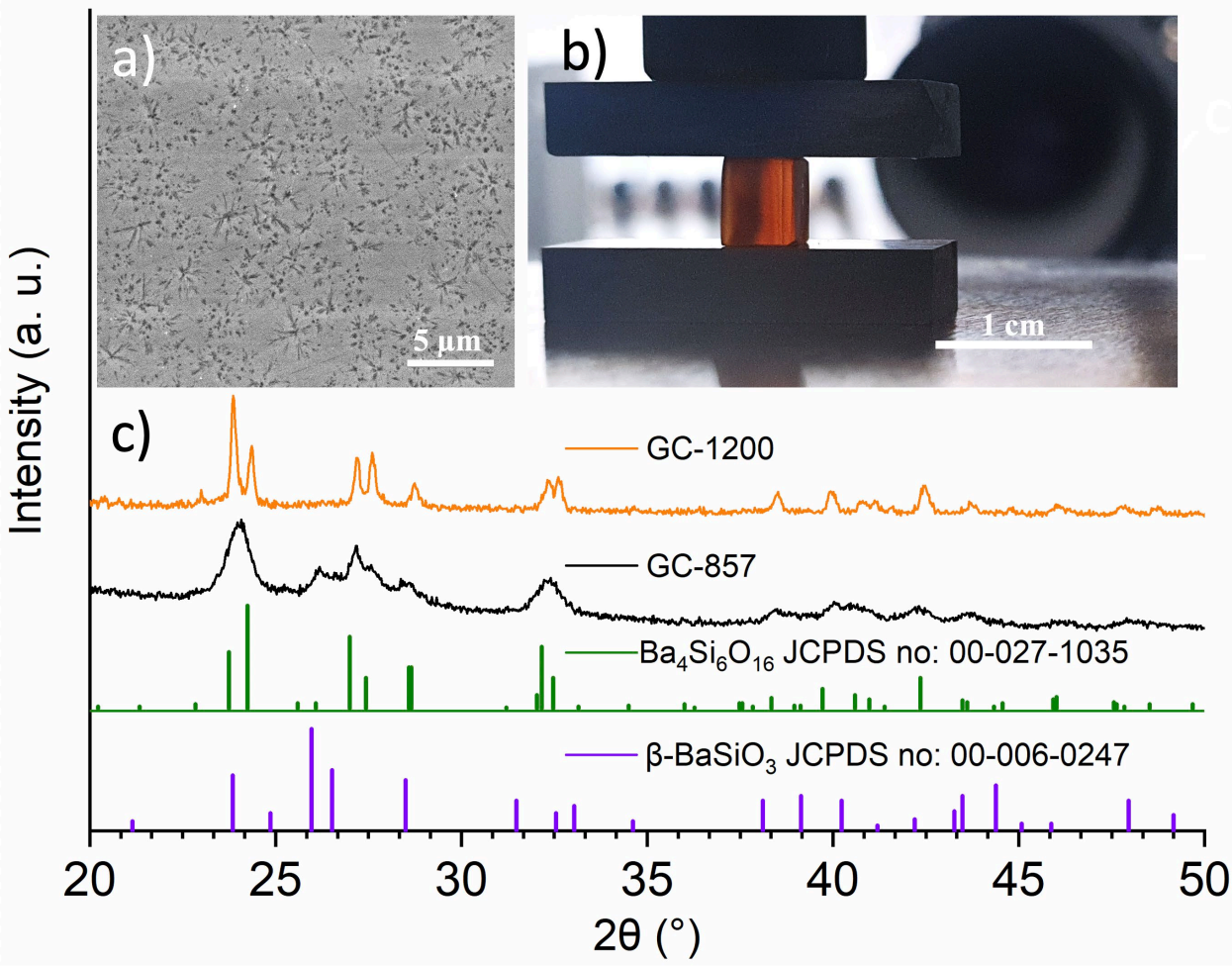

FIG. 2. a) *SEM* micrograph of GC-857 b) Photograph of the experimental setup with GC-857 c) *XRD* patterns of GC-1200 (orange), GC-857 (black), $Ba_4Si_6O_{16}$ (green) and β-$BaSiO_3$ (purple).

Different heat-treatment temperatures and durations were investigated in order to develop glass-ceramics with different levels of transparency and different fraction of crystallized phases with a direct incidence on the mechanoluminescence intensity. The main outcomes of these lengthy experimental campaigns is that, on the one side, a heat-treatment of 3 h at T_g+20 °C (sample GC-857) allows to observe mechanoluminescence while maintaining the transparency of the glass-ceramic (Fig. 2b), whereas on the other side heat-treatments at higher temperature lead to a more intense

mechanoluminescence response but to opaque yellowish/greenish samples. In this latter case, an optimum was observed for a heat-treatment of 10 min. at 1200 °C, that is well above the crystallization temperature but below the melting temperature of $Ba_4Si_6O_{16}$ (sample GC-1200). Longer treatment times were found to induce the degradation of the surface of the material (a few tens of microns porous layer forms at the surface). The major crystalline phase in the glass-ceramics as identified by means of *XRD* on powders (after grounding the glass-ceramics) is $Ba_4Si_6O_{16}$ (space group $P2_1/c$) (Fig. 2c). This confirms the congruent crystallization of the glass. The presence of a minor amount of β-$BaSiO_3$[27] in GC-857 is attributed to a side surface crystallization process. The amount of residual glassy phase in GC-857 remains important according to the width of the *XRD* peaks and to the *SEM* micrograph, where the glassy phase (light grey) is dominant. In the case of GC-1200, well-defined peaks corresponding to the $Ba_4Si_6O_{16}$ phase are observed and the material is almost fully crystallized.

Non-destructive elastico-mechanoluminescence was observed by loading parallelepipedic glass-ceramic specimens in compression at a rate of 300 MPa·s^{-1}. The specimens were *UV*-irradiated prior to testing and mechanically loaded 4 and 30 s later for the GC-857 and GC-1200 grades respectively (Fig. 3). The mechanoluminescence intensity was obtained by subtracting the photoluminescence decay background as obtained on the same specimen in the absence of mechanical loading. The mechanoluminescence intensity gradually decreases i) with increasing delay times before applying the mechanical stress ii) during cyclic compression tests (Supplementary data 1). This suggests that the charge carriers involved in the mechanoluminescence mechanisms are slowly recombining with the luminescent centers with time, but also that mechanical stress increases the recombination kinetics. For a given loading rate, an increase of the intensity of the mechanoluminescence peak is observed with an increase of the maximum stress, consistently with the fact that as the applied stress is increased the release of the charge carriers becomes easier (faster)[1,10]. Then, the mechanoluminescence intensity decreases continuously during the stress plateau. Mechanoluminescence is more pronounced in GC-1200 than in GC-857 thanks to a larger fraction of "active" crystallized phase, and can thus be detected in GC-1200 even at relatively low loading rates. As a result, the weakening of the mechanoluminescence phenomenon during the unloading stage is easier to follow (Fig. 3b). As far as mechanoluminescence is under scrutiny, the loading-rate is of paramount importance. The mechanoluminescence intensity was found previously in the case of the $SrAl_2O_4:Eu^{2+}$, Dy^{3+} compound to be proportional to the mechanical power, $P_m = \frac{\sigma\dot{\sigma}}{E}$, where $\dot{\sigma}$ is the stress-rate and E the Young's modulus of the material[1]. However, the mechanoluminescence behavior of $Ba_4Si_6O_{16}:Eu^{2+}$, Ho^{3+} differs from the one of $SrAl_2O_4:Eu^{2+}$, Dy^{3+} in that the luminescence intensity drops rapidly upon unloading. In the case of $SrAl_2O_4:Eu^{2+}$, Dy^{3+}, a

mechanism for the mechanoluminescence based on the existence of three discreet trap levels in the crystal structure was proposed and sustained by experiments conducted in hydrostatic pressure, in compression and in shear and by *DFT* calculations[1,2].

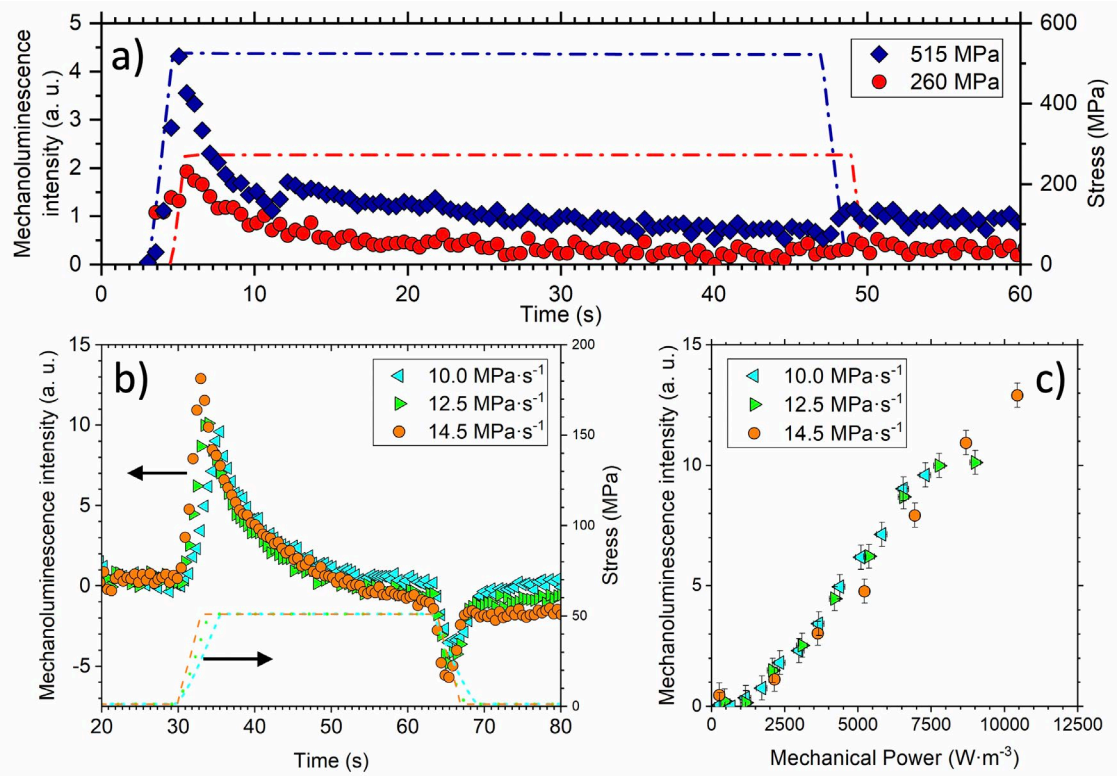

FIG. 3. a) Mechanoluminescence behavior of the GC-857 glass-ceramics under different stress condition: b) Mechanoluminescence behavior of the GC-1200 glass-ceramics for loading cycles with different loading and unloading rates c) Mechanoluminescence intensity as a function of the mechanical power for the GC-1200 glass-ceramics.

In $Ba_4Si_6O_{16}:Eu^{2+}$, Ho^{3+}, defects such as oxygen vacancies are likely to play an important role in the luminescence and mechanoluminescence mechanisms. There are eight non-equivalent oxygen sites in the corresponding crystal structure. Therefore, eight models were investigated by means of *DFT* to account for the effect of creating a specific oxygen vacancy in a $Ba_4Si_6O_{16}$ crystal. Nevertheless, these eight possible configurations lead (after optimization) to only two types of local atomic arrangement at the defect sites,, which are associated with the two types of oxygen atoms, namely those internal with respect to the silicate ribbon, and those external (Fig. 4b). While the external oxygen atoms are connected to only one silicon atom, the internal ones are bonded to two silicon atoms. As a consequence, the formation of an oxygen vacancy is more favorable on the edges of the ribbon (O_1, O_2, O_5 and O_7) than inside the ribbon (O_3, O_4, O_6 and O_8), and leads to SiO_3 and Si_2O_6 entities, respectively. It is interesting to notice that the latter defect exhibits Si-Si distances of 2.59, 2.58, 2.49 and 2.44 Å, respectively for V_{O3}, V_{O4}, V_{O6} and V_{O8}, for which the relative energies are 792, 816, 1050, and 1209 meV, respectively. In other words, the formation of oxygen vacancies

inside the ribbon is clearly unfavorable and a shorter Si-Si distance leads to increase the instability of the related Si_2O_6 defect. The incidence of the eight different oxygen vacancies on the density of states (*DOS*) was evaluated and is shown in Fig. 4 along with the *DOS* of the defect-free supercell. A band gap value of 4.7 eV is found, similar to the one reported by Li et al. (4.6 eV) [12]. Both deep and shallow defect levels originating from the removal of the oxygen atom were identified. Unlike the case of $SrAl_2O_4$ [2], the shallow defect levels of $Ba_4Si_6O_{16}$ are rather diffuse. This is believed to have a strong incidence on the mechanoluminescence behavior of this crystal. Nevertheless, further experimental and theoretical investigations are needed to reach a complete understanding of the response of the $Ba_4Si_6O_{16}:Eu^{2+}$, Ho^{3+} compound to a specific mechanical loading cycle.

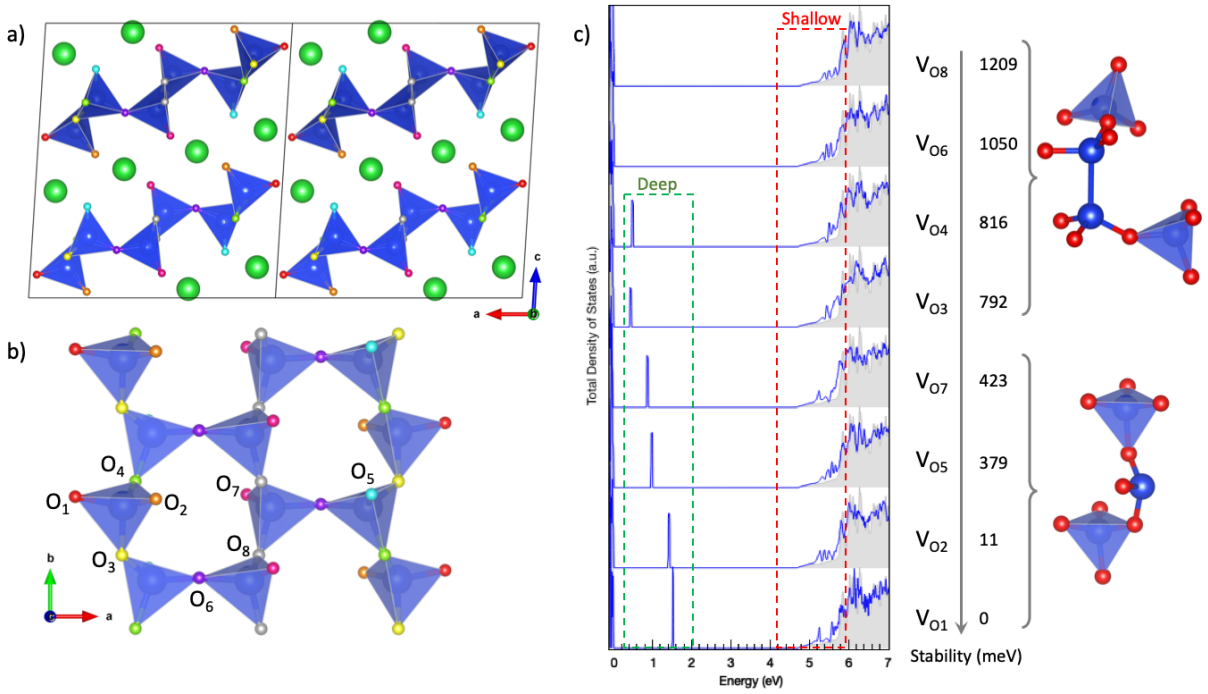

FIG. 4. a) Schematic representation of the atomic structure of $Ba_4Si_6O_{16}$, which is built on ribbons of corner-sharing SiO_4 tetrahedra (in blue) separated from each other by Ba^{2+} ions (in green). b) The eight inequivalent oxygen positions in a ribbon can be classified in two categories, namely external (O_1, O_2, O_5 and O_7) and internal (O_3, O_4, O_6 and O_8) to ribbon. c) The total densities of states (*TDOS*) corresponding to formation of an oxygen vacancy containing one electron (blue line) on each inequivalent oxygen sites (V_{Oi}) are compared to the defect-free *TDOS* (in grey). Energies for *TDOS* are given with respect to the E_F. Deep and shallow defect energy range regions with respect to the conduction band are highlighted. The relative energy, i.e. the related stability of the defect, is given in meV. The atomic arrangements resulting from the removing of external and internal oxygen atoms are shown.

In conclusion, mechanoluminescence was observed in glass-ceramics from the $BaO\text{-}SiO_2\text{-}Si_3N_4$ chemical system containing 4 mol. % (EuO, Ho_2O_3). The crystallized phase of interest, e.g.

$Ba_4Si_6O_{16}:Eu^{2+}$, Ho^{3+}, was obtained through a congruent crystallization of a glass with the same composition. Large (cm scale) batches of homogeneous parent glasses and glass-ceramics were elaborated. The intensity of the mechanoluminescence response observed after loading, post-*UV* irradiation, scales with the mechanical power (i.e. with the loading-rate). However, some major differences were noticed with the behavior of $SrAl_2O_4:Eu^{2+}$, Dy^{3+}, which result from the differences in the energy levels induced by the oxygen vacancies.

We acknowledge financial support from Région Bretagne (ARED grant) and from the European Research Council (ERC Adv. Grant 320506 “DAMREG”).

ORCID

Alexis Duval iD https://orcid.org/0000-0001-9192-2454
Patrick Houizot iD https://orcid.org/0000-0002-6360-6996
Xavier Rocquefelte iD https://orcid.org/0000-0003-0191-2354
Tanguy Rouxel iD https://orcid.org/ 0000-0002-9961-2458

REFERENCES

[1] M. Dubernet, Y. Gueguen, P. Houizot, F. Célarié, J.C. Sangleboeuf, H. Orain, and T. Rouxel, Appl. Phys. Lett. **107**, 151906 (2015).
[2] M. Dubernet, E. Bruyer, Y. Gueguen, P. Houizot, J.C. Hameline, X. Rocquefelte, and T. Rouxel, Sci. Rep. **10**, 1 (2020).
[3] Y. Xie and Z. Li, Mater. Chem. Front. **4**, 317 (2020).
[4] A. Feng and P.F. Smet, Materials (Basel). **11**, 484 (2018).
[5] T. Matsuzawa, Y. Aoki, N. Takeuchi, and Y. Murayama, J. Electrochem. Soc. **143**, 2670 (1996).
[6] C.N. Xu, T. Watanabe, M. Akiyama, and X.G. Zheng, Appl. Phys. Lett. **74**, 2414 (1999).
[7] Y. Zhuang and R.J. Xie, Adv. Mater. **33**, 1 (2021).
[8] J. Cao, Y. Ding, R. Sajzew, M. Sun, F. Langenhorst, and L. Wondraczek, Opt. Mater. Express **12**, 3238 (2022).
[9] Z. Feng, J. Zhang, X. Xu, T. Zheng, Y. Guo, and J. Lv, J. Non. Cryst. Solids **590**, 121676 (2022).
[10] J. Botterman, K. Van Den Eeckhout, I. De Baere, D. Poelman, and P.F. Smet, Acta Mater. **60**, 5494 (2012).
[11] T. Ishihara, K. Tanaka, K. Fujita, K. Hirao, and N. Soga, Solid State Commun. **107**, 763 (1998).
[12] Y. Li, Y. Fang, N. Hirosaki, R.J. Xie, L. Liu, T. Takeda, and X. Li, Materials (Basel). **3**, 1692 (2010).
[13] M. Chen, Z. Xia, M.S. Molokeev, and Q. Liu, J. Mater. Chem. C **3**, 12477 (2015).
[14] W.-S. Song, H.-J. Kim, Y.-S. Kim, and H. Yang, J. Electrochem. Soc. **157**, J319 (2010).
[15] Z. Yang, Y. Hu, L. Chen, and X. Wang, Opt. Mater. (Amst). **35**, 1264 (2013).
[16] R.D. Shannon, Acta Crystallogr. Sect. A **32**, 751 (1976).
[17] J. Moriceau, P. Houizot, T. To, A. Mougari, H. Orain, F. Celarié, and T. Rouxel, J. Eur. Ceram. Soc. **41**, 838 (2021).
[18] A. Duval, P. Houizot, and T. Rouxel, J. Am. Ceram. Soc. **106**, 1611 (2022).
[19] N. Claussen and J. Jahn, Powder Metall. Inernational **2**, 87 (1970).
[20] K.-F. Hesse and F. Liebau, Zeitschrift Für Krist. **153**, 3 (1980).

[21] G. Kresse and J. Hafner, Phys. Rev. B **48**, 13115 (1993).
[22] G. Kresse and J. Furthmüller, Phys. Rev. B **54**, 11169 (1996).
[23] J.P. Perdew, K. Burke, and M. Ernzerhof, Phys. Rev. Lett. **77**, 3865 (1996).
[24] R. Ramesh, E. Nestor, M.J. Pomeroy, and S. Hampshire, J. Eur. Ceram. Soc. **17**, 1933 (1997).
[25] D. de Graaf, H.T. Hintzen, S. Hampshire, and G. de With, J. Eur. Ceram. Soc. **23**, 1093 (2003).
[26] M.W. Chase, J. Phys. Chem. Ref. Data 1 (1998).
[27] R.J.M. Konings, O. Beneš, A. Kovács, D. Manara, D. Sedmidubskỳ, L. Gorokhov, V.S. Iorish, V. Yungman, E. Shenyavskaya, and E. Osina, J. Phys. Chem. Ref. Data **43**, (2014).
[28] D.R. Messier and E.J. Deguire, J. Am. Ceram. Soc. **67**, 602 (1984).
[29] H.D. Batha and E.D. Whitney, J. Am. Ceram. Soc. **56**, 365 (1973).
[30] L.A. Gorelova, R.S. Bubnova, S. V. Krivovichev, M.G. Krzhizhanovskaya, and S.K. Filatov, J. Solid State Chem. **235**, 76 (2016).

SUPPLEMENTARY DATA

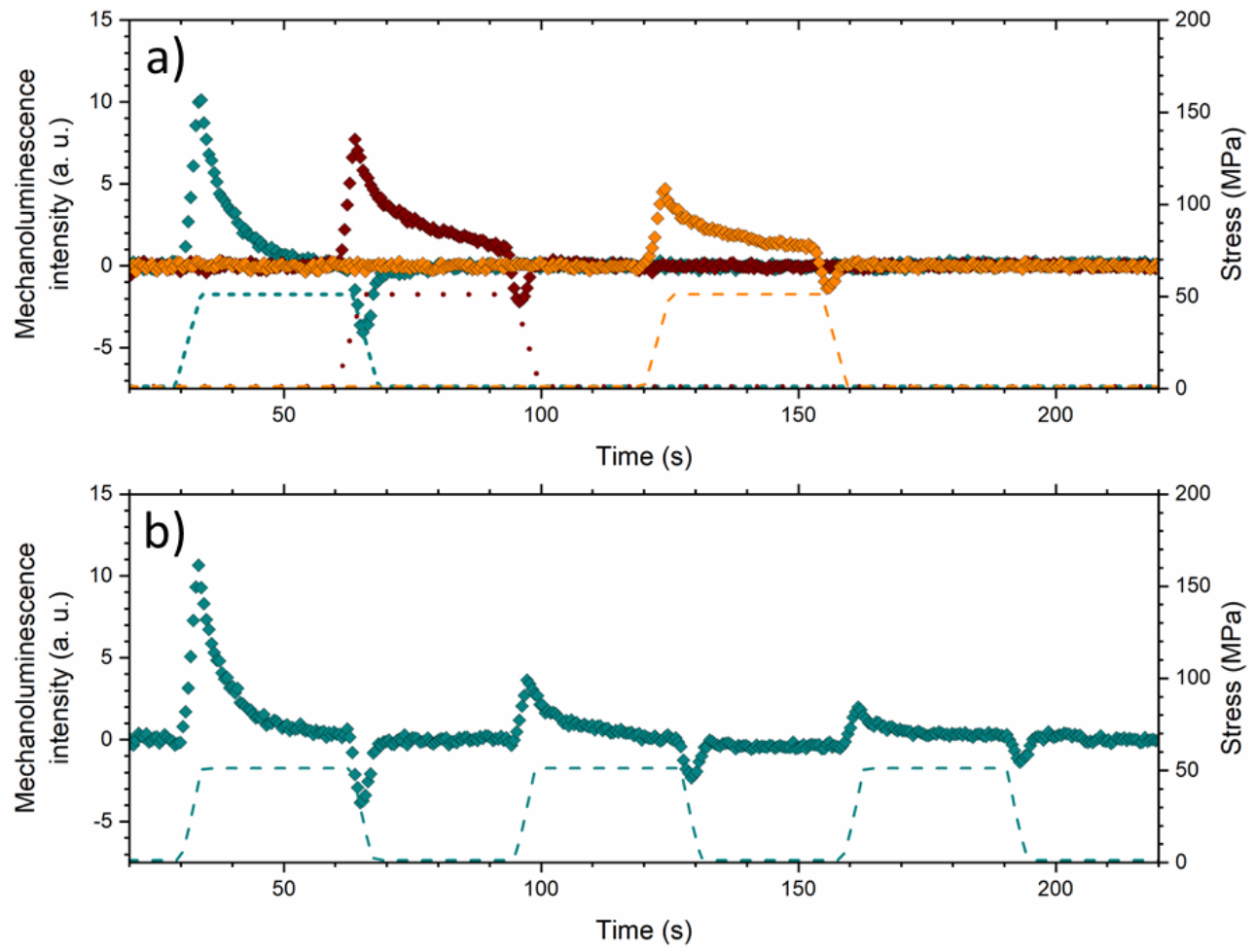

SUPPLEMENTARY DATA 1. a) Mechanoluminescence of GC-1200 a) with different delay times before applying the load b) under cyclic compression tests.